PHYSICAL REVIEW D **89,** 124020 (2014)

Lifshitz black holes in Einstein-Yang-Mills theory

Deniz Olgu Devecioğlu[*]

Department of Physics, Faculty of Arts and Sciences, Middle East Technical University, 06800 Ankara, Turkey

(Received 28 January 2014; published 16 June 2014)

We find that the four-dimensional cosmological Einstein-Yang-Mills theory with $SU(2)$ gauge group admits Lifshitz spacetime as a base solution for the dynamical exponent $z > 1$. Motivated by this, we next demonstrate numerically that the field equations admit black hole solutions which behave regularly on the horizon and at spatial infinity for different horizon topologies. The solutions depend on one parameter, the strength of the gauge field at the horizon, which is fine-tuned to capture the Lifshitz asymptotics at infinity. We also discuss the behavior of solutions and the change in Hawking temperature for black holes that are large or small with respect to the length scale L, which is itself fixed by the value of the cosmological constant.

DOI: 10.1103/PhysRevD.89.124020 PACS numbers: 04.70.Bw, 04.25.dg, 04.70.-s

I. INTRODUCTION

The AdS/CFT conjecture has been a strong and versatile tool in the arsenal of high energy theory. The aptly named duality, relating conformal field theories to gravity in higher dimensions, has proven to be a powerful theoretical toolkit and provided great insight in high energy physics. Recently, there has been a serious effort to trickle down to the energy scale of condensed matter and make holography accessible to strongly coupled systems which can be realized in experiments [1–4] (and references therein). One of the approaches to achieve such duality is to impose an anisotropic scaling symmetry on the boundary field theory

$$t \to \lambda^z t, \qquad \vec{x} \to \lambda \vec{x}, \qquad r \to \frac{r}{\lambda}, \tag{1}$$

where z is called the dynamical exponent. The symmetry algebra of field theories is controlled by z, e.g., $z = 1$ generates the Poincaré group with special conformal symmetries, and when $z > 1$, one ends up with different scalings for time and space, which leads to nonrelativistic field theories with Lifshitz symmetries: our main focus in this work. The bulk metric conjuring up these symmetries is found to be

$$ds^2 = L^2\left(-r^{2z}dt^2 + \frac{dr^2}{r^2} + r^2 d\vec{x}^2\right), \tag{2}$$

with peculiar properties regarding causal structure and geodesics [2,5]. Einstein gravity with a negative cosmological constant does not admit this type of anisotropic background as a solution. One should either consider higher derivative theories or matter couplings to source the metric. Once we depart from Einstein gravity and add the higher curvature corrections, the amended theories begin to accommodate (2) as a solution [6]. On the other hand, the anisotropic backgrounds engineered with various types of matter Lagrangians [7]—e.g., string theory motivated p-form fields [5], massive gauge fields, and $U(1)$ fields with dilatoniclike couplings [8]—are better studied models for gravity duals. One of the first examples is the theory considered in [5], which is conjectured to be the gravitational dual of $2+1$ dimensional field theories modeling quantum critical behavior in strongly correlated electron systems.

In principle, black hole solutions describe the finite temperature behavior of those dual nonrelativistic field theories, which renders them important objects in holography. Curvature corrections open up the way for large families of analytic black holes in different dimensions, both for static and stationary Lifshitz spacetimes [6,9–11]. However, analytic black holes with matter fields for generic z are rather rare [7,8]. For a fixed value of z, several exact solutions were found [12–15]. On the other hand, different types of numerical solutions were explored with generic z values and for different horizon topologies [16–20] for theories with massive gauge fields and p forms.

The matter Lagrangians with non-Abelian gauge fields have been used in holographic superconductor models [21,22], with AdS/Schwarzschild black hole backgrounds. Recently, the effects of Lifshitz scaling on these models have also been considered [23]. In this work we will first focus on a different and simpler question: whether it is possible at all to support Lifshitz spacetime (2) with non-Abelian matter sources. To our knowledge, this has not been addressed previously elsewhere. Having answered the first in the affirmative, the second task we undertake is the dressing up of this background solution with black holes. There is substantial literature on Einstein-Yang-Mills particlelike and black hole solutions [24–28], both in

[*]dedeveci@metu.edu.tr

asymptotically flat and AdS backgrounds with different characteristics. For example, asymptotically flat, colored black holes [25] admit finite range field strength; i.e., there is no global magnetic $SU(2)$ charge that makes them indistinguishable from Schwarzschild at infinity, whereas asymptotically AdS ones can possess global $SU(2)$ magnetic charge [28]. As we will show in what follows, Lifshitz asymptotics are quite different: Fields extend to infinity not only to endow black holes with $SU(2)$ charge, but also to support Lifshitz spacetime. By abandoning asymptotic flatness, black holes with nonspherical horizon topologies can be constructed. Accordingly, we will consider three types of event horizon topologies—viz., planar, spherical, and hyperbolic—with different gauge field Ansätze respecting the corresponding symmetries.

For large black holes, these three types have similar behavior but differ significantly in the case of small event horizon radii. Our focus will be on the numerical evidence for the asymptotically Lifshitz black holes in cosmological Einstein-Yang-Mills (EYM) theory. We will not discuss the relation to the holographic dual field theories, which merits a separate significant problem on its own.

The outline of the paper is as follows: In Sec. II we start with the equations of motion for the EYM system, state the Ansatz for the planar symmetric Yang-Mills (YM) fields, and obtain the solution for the background metric (2). We then set the stage for black hole solutions by dressing up the background metric and gauge fields with suitable functions in Sec. III. Sections IV A and IV B are devoted to the series solutions of black holes at infinity and at the horizon, respectively. We next study the numerical black hole solutions of the theory in Sec. IV C. In Sec. V the Hawking temperature of the solutions we have found is analyzed. Finally, we conclude with Sec. VI.

II. LIFSHITZ ASYMPTOTICS AND $SU(2)$ GAUGE FIELDS

The gravity theory we consider is the four-dimensional cosmological EYM theory for the gauge group $SU(2)$, described by the action

$$S=\int d^4x\sqrt{-g}\left((R-2\Lambda)-\frac{1}{2g_{\rm YM}^2}{\rm Tr}F_{\mu\nu}F^{\mu\nu}\right), \quad (3)$$

where Λ is the cosmological and $g_{\rm YM}^2$ is the gauge coupling constant in dimensions of $1/\text{length}^2$.[1] In order to support backgrounds with anisotropic scaling symmetry, a naive approach is to make the coupling constants depend on the geometry, i.e., the parameter z. It is worth emphasizing that the path taken here is different from [28,29], in which AdS is already a vacuum for the gravitational sector and the YM field is used only as a hair parameter, not for supporting the AdS geometry. In this work the YM field will be used to source the metric (2), so it has to decouple at $z=1$. Because of this major difference, we will not be able to recover the results of [28] in the conformal limit $z=1$. As we will show in the discussion below, ours is still an appropriate way to proceed.

Einstein field equations following from the action (3) read

$$R_{\mu\nu}-\Lambda g_{\mu\nu}=\frac{1}{g_{\rm YM}^2}T_{\mu\nu}, \quad (4)$$

with the traceless YM stress-energy tensor defined as

$$T_{\mu\nu}\equiv{\rm Tr}\left(F_\mu{}^\alpha F_{\nu\alpha}-\frac{1}{4}g_{\mu\nu}F_{\alpha\beta}F^{\alpha\beta}\right), \quad (5)$$

and the YM field equations

$$D_\mu F^{\mu\nu}=0, \quad (6)$$

where the gauge covariant derivative is defined as $D_\mu\equiv\nabla_\mu-i[A_\mu,\,]$.

The traceless nature of the stress-energy tensor allows us to determine the value of the cosmological constant from Einstein field equations. The trace of (4) when used with the metric (2) yields

$$\Lambda=-\frac{3+2z+z^2}{2L^2}. \quad (7)$$

The next step is to consider the non-Abelian gauge field configuration respecting the symmetry of the plane, which is a subgroup of the Poincaré group and is studied extensively in [30,31]. Additionally, we shall also restrict ourselves to the static and purely magnetic case. This restriction leads to the $SU(2)$ gauge connection

$$A_\mu dx^\mu=w(r)T^1dx_1+w(r)T^2dx_2. \quad (8)$$

For our purposes, it is convenient to express the metric (2) in a form which is analogous to the one that is commonly used[2] (see Refs. [26–28]):

$$ds^2=L^2\left(-S(r)^2\mu(r)dt^2+\frac{dr^2}{\mu(r)}+r^2d\vec{x}^2\right). \quad (9)$$

[1]Here $F_{\mu\nu}$ is the gauge field strength $F_{\mu\nu}\equiv F_{\mu\nu}^aT_a=\partial_\mu A_\nu-\partial_\nu A_\mu-i[A_\mu,A_\nu]$ and we choose generators $T_a\equiv\tau_a/2$ and $a=1,2,3$, with τ_a denoting Pauli matrices. The commutation relations and the normalization of generators are given as $[T_a,T_b]=i\epsilon_{abc}T_c$ and ${\rm Tr}T_aT_b=\delta_{ab}/2$, respectively. Throughout, we use the conventions in which the signature of metrics is $(-,+,+,+)$, with the Riemann tensor taken as $R^\mu{}_{\nu\alpha\beta}=\partial_\alpha\Gamma^\mu{}_{\beta\nu}-\cdots$ and $R_{\mu\nu}=R^\alpha{}_{\mu\alpha\nu}$.

[2]Here we are considering the planar case, whereas in the literature the spatial part of (9) is typically spherical, with a different gauge field Ansatz. The other cases can also be treated in a similar manner, which will be discussed later in the next section.

Taking (8) and (9) into account, field equations (4) and (6) reduce to the system

$$S^{-1}S' = \frac{1}{2L^2 g_{\rm YM}^2}\frac{(w')^2}{r}, \tag{10}$$

$$(\mu w')' = \frac{w^3}{r^2} - \frac{1}{2L^2 g_{\rm YM}^2}\frac{\mu (w')^3}{r}, \tag{11}$$

$$r\mu' + \mu + L^2 r^2 \Lambda = -\frac{1}{2g_{\rm YM}^2 L^2}\left(\frac{w^4}{2r^2} + \mu (w')^2\right), \tag{12}$$

with primes denoting the ordinary derivative with respect to r.

Plugging in $S(r) = r^{z-1}$ and $\mu(r) = r^2$ and using (7), it is straightforward to show that Lifshitz spacetime (2) is a solution for all $z > 1$, provided that the gauge field and the coupling constant are chosen as

$$w(r) = \pm\sqrt{z+1}\, r, \qquad g_{\rm YM}^2 = \frac{1}{2L^2}\frac{(z+1)}{(z-1)}. \tag{13}$$

The sign ambiguity of the gauge field can be deduced from the invariance of the field equations (10), (11), and (12) under $w(r) \to -w(r)$, which corresponds to a gauge transformation [27]. Hence, in what follows we will proceed with the positive sign gauge field. The solution we have found is basically a "colorful plane with Lifshitz asymptotics." Note also that $z > 1$ in order to have real gauge fields, which signals the "critical slowing down" of the possible dual field theories [5].

The conformal limit $z \to 1$ of (13) is also peculiar. The YM part decouples from the gravity action and, as is well known, AdS spacetime is a solution of (4) without matter fields, provided $\Lambda = -3/L^2$. Moreover, the decoupled gauge field is a solution to the pure YM part, which is in some sense the AdS analogue of the flat space solution given in [30,31].

Having determined that the non-Abelian YM matter is suitable for Lifshitz asymptotics, we can now continue and dress up this background geometry to obtain black hole solutions.

III. FIELD EQUATIONS

In this section we first extend the metric and the gauge field Ansatz to cover the other types of event horizon topologies, then cast the field equations in a way that is convenient for capturing the Lifshitz asymptotics for both the metric and the gauge field at large spatial distance.

We will control the spatial part of the metric by introducing a parameter k,

$$ds^2 = L^2\left(-S(r)^2\mu(r)dt^2 + \frac{dr^2}{\mu(r)} + r^2 d\Omega_k^2\right), \tag{14}$$

where

$$d\Omega_k^2 \equiv \begin{cases} d\theta^2 + \sin^2\theta d\phi^2 & k = +1 \\ d\theta^2 + \sinh^2\theta d\phi^2 & k = -1 \\ d\theta^2 + d\phi^2 & k = 0. \end{cases} \tag{15}$$

It is clear from this definition that $k = 0$ corresponds to the planar symmetric case we have discussed previously, $k = 1$ yields the spherically symmetric metric, and the $k = -1$ option is invariant under hyperbolic rotations.

The gauge field Ansatz will change accordingly by taking into account the symmetries of the metric (15). It is well known that the isometries of spacetime follow from the Lie derivative of the metric $g_{\mu\nu}$,

$$\mathcal{L}_{\xi_m} g_{\mu\nu} = 0, \tag{16}$$

where ξ_m's are the set of Killing vectors generating isometries. Intuitively, the condition for a spacetime symmetric gauge field $A_\mu(x)$ can be defined as

$$\mathcal{L}_{\xi_m} A_\mu = 0. \tag{17}$$

However, there is even more to the story: There is a gauge transformation freedom in infinitesimal form $A'_\mu(x) = A_\mu(x) + \epsilon D_\mu W$, where ϵ is a small parameter and $W = W(x)^a T^a$ is a function in the Lie algebra of the gauge group. With this transformation freedom, the symmetry condition for a gauge field reads [32,33]

$$\mathcal{L}_{\xi_m} A_\mu = D_\mu W_m, \tag{18}$$

from which the integrability conditions that are used to determine W_m's can be obtained. Eventually, by solving (18), the most general form of the spacetime symmetric A_μ can be found.

The plane symmetric gauge field Ansatz used in the previous section follows from this procedure. In addition to that, we will also consider the following static $SU(2)$ connections that are invariant under $SO(3)$ (which is known as the Witten Ansatz) and the connected part of $SO(2,1)$ [32,34],

$$\begin{aligned} A = {} & q(r)T^3 dt + p(r)T^3 dr + (w(r)T^1 + u(r)T^2)d\theta \\ & + (w(r)\Omega_k(\theta)T^2 - u(r)\Omega_k(\theta)T^1 + \tilde{\Omega}_k(\theta)T^3)d\phi, \end{aligned} \tag{19}$$

for $k = 1, -1$, where $\Omega_1(\theta) \equiv \sin\theta, \Omega_{-1}(\theta) \equiv \sinh\theta$, $\tilde{\Omega}_1(\theta) \equiv \cos\theta$, and $\tilde{\Omega}_{-1}(\theta) \equiv \cosh\theta$.

This expression still has a $U(1)$ gauge freedom [26], which can be used to set $u(r) = 0$. Next, with the help of the field equations, we see that $p(r) = 0$, provided that $w(r) \neq 0$. In order to simplify the discussion, we will only consider the gauge field strengths with a vanishing electric

part, i.e., $q(r) = 0$. In fact this choice is rather restrictive. It was shown in [35] that, with appropriate asymptotics, the Reissner-Nordström solution is the only static black hole with a nonzero YM electric field. However, all of this was for asymptotically flat backgrounds and, obviously, these arguments do not necessarily apply for Lifshitz spacetimes. Nevertheless, we shall restrict ourselves to the purely magnetic Ansatz in this work.

Taking these considerations into account, we are thus led to

$$A = \begin{cases} w(r)T^1 d\theta + (w(r)\Omega_k(\theta)T^2 + \tilde{\Omega}_k(\theta)T^3)d\phi & \text{for } k = \pm 1 \\ w(r)T^1 d\theta + w(r)T^2 d\phi & \text{for } k = 0. \end{cases} \tag{20}$$

Now, utilizing the generalized metric (14) and the gauge field Ansatz (20), Eqs. (10), (11), and (12) can be cast into a general form covering all possible cases [29]:

$$S^{-1}S' = \frac{1}{2L^2 g_{\rm YM}^2}\frac{(w')^2}{r}, \tag{21}$$

$$(\mu w')' = \frac{w(w^2-k)}{r^2} - \frac{1}{2L^2 g_{\rm YM}^2}\frac{\mu (w')^3}{r}, \tag{22}$$

$$r\mu' + \mu + L^2 r^2 \Lambda - k = -\frac{1}{2g_{\rm YM}^2 L^2}\left(\frac{(w^2-k)^2}{2r^2} + \mu (w')^2\right). \tag{23}$$

Although this form of the field equations is helpful for exploring the constraints on the functions at the horizon, it is a bit impractical for numerical purposes. It is more appropriate to redefine the metric and the gauge field functions such that the Lifshitz vacuum (2) can be explicitly recovered at large radii. One can achieve this with simple redefinitions

$$w(r) \equiv \sqrt{z+1}\, r h(r), \qquad \mu(r) \equiv \frac{r^2}{g(r)^2}, \\ S(r) \equiv r^{z-1} f(r) g(r), \qquad w'(r) \equiv \sqrt{z+1}\, j(r). \tag{24}$$

It is obvious from these definitions that if all the unknown functions $f(r)$, $g(r)$, $h(r)$, and $j(r)$ are one in the large r limit (i.e., when $r \gg 1$), then we recover the Lifshitz background solution we have constructed for the EYM system, with $k = 0$.

All of these assumptions and identifications and the coupling constants (7) and (13) yield the following system of equations:

$$rf(r)' = -f(r)\left((z-1) - \frac{j(r)^2}{2}(z-1) + \frac{g(r)^2 h(r)^4}{4}(z^2-1) - \frac{g(r)^2}{4}(3+2z+z^2) + \frac{3}{2}\right) \\ - kf(r)g(r)^2\left\{\frac{k}{4r^4}\frac{(z-1)}{(z+1)} - \frac{h(r)^2}{2r^2}(z-1) - \frac{1}{2r^2}\right\}, \tag{25}$$

$$rj(r)' = j(r) + g(r)^2 h(r)^3 (z+1) - \frac{g(r)^2 j(r)}{2}(z^2+2z+3) + \frac{g(r)^2 h(r)^4 j(r)}{2}(z^2-1) \\ - k\left\{g(r)^2\left(\frac{h(r)^2 j(r)}{r^2}(z-1) - k\frac{j(r)}{2r^4}\frac{(z-1)}{(z+1)} + \frac{j(r)}{r^2} + \frac{h(r)}{r^2}\right)\right\}, \tag{26}$$

$$rg(r)' = \frac{g(r)j(r)^2}{2}(z-1) + \frac{g(r)^3 h(r)^4}{4}(z^2-1) - g(r)^3(3+2z+z^2) + \frac{3g(r)}{2} \\ + kg(r)^3\left\{\frac{k}{4r^4}\frac{(z-1)}{(z+1)} - \frac{h(r)^2}{2r^2}(z-1) - \frac{1}{2r^2}\right\}, \tag{27}$$

$$rh(r)' = j(r) - h(r). \tag{28}$$

Several observations are in order here. The highly nonlinear nature of the EYM system makes the analytic study difficult and, despite our efforts, we could not find an exact solution with nontrivial gauge field functions. Yet it is simple enough for working numerically since we have reduced the system into one of coupled first-order ordinary differential equations, with the functions having definite asymptotic values.

Second, terms explicitly involving $1/r^2$ and $1/r^4$ appear only in spherical and hyperbolic cases where $k = \pm 1$. Exploiting this fact, we will assume that in the large r limit, the spherical and hyperbolic spatial parts can be replaced by a flat one [16] [20]. Thus all of the unknown functions appearing in the numerical solutions will have the same asymptotic behavior, i.e., $f(r) = g(r) = h(r) = j(r) = 1$.

Note that the three equations (26)–(28) form a closed system on their own, and Eq. (25) can be considered separately. In addition, the right-hand side of (25) is linear in the function $f(r)$, which makes its normalization undetermined. This leads to a scaling of the initial value of f at large r, which is essentially a gauge choice, i.e., a rescaling of the time coordinate [5]. In order to get the correct asymptotics after the numerical integration, proper initial values must be chosen.

We now need to expand the functions $f(r), g(r), h(r),$ and $j(r)$, at large r and separately at the horizon, for all possible values of the parameter k but for a fixed value of z. One can extract a shooting parameter from the asymptotic form of the solutions to (25), (26), (27), and (28) provided there is one available with the given boundary conditions; this is of paramount importance for the numerical study.

IV. SERIES AND NUMERICAL SOLUTIONS

We now describe the results obtained by expanding the functions at large radii and at the horizon, whose existence we presume. The series solution will teach us a great deal about the initial values and bounds on the functions defined in the previous section. We will then consider the numerical solutions of the system for various cases.

A. Series solution for the large radius

First we look for the series solutions at large r, which in principle can confirm the plausibility of the assumption we have made in regards to the employment of the planar background for all horizon types at large r. The behavior of solutions is rather interesting for different values of z. It turns out that geometries with even integer dynamical exponent z admit only planar solutions. However, all types of geometries are supported when z is chosen to be an odd integer. In order to establish this result, we first fix the value of z in Eqs. (25), (26), (27), and (28), then make a simple transformation $r = 1/x$, and finally assume a power series expansion at small x,

$$f(r) = \sum_{n=0}^{\infty} \tilde{f}_n x^n, \qquad g(r) = \sum_{n=0}^{\infty} \tilde{g}_n x^n,$$
$$h(r) = \sum_{n=0}^{\infty} \tilde{h}_n x^n, \qquad j(r) = \sum_{n=0}^{\infty} \tilde{j}_n x^n, \tag{29}$$

with the Lifshitz asymptotics (i.e., $\tilde{f}_0 = \tilde{g}_0 = \tilde{h}_0 = \tilde{j}_0 = 1$). We insert these into the equations of motion (25), (26), (27), and (28) and work order by order in x. We can summarize our findings as follows[3]:

For $z = 2$ and $k = 0$, we find

$$f(r) = 1 - \frac{9h_L}{2r^4} - \frac{1557}{176}\frac{h_L^2}{r^8} + \mathcal{O}(1/r^{16}) + \cdots, \tag{30}$$

$$g(r) = 1 + \frac{6h_L}{r^4} + \frac{1143}{22}\frac{h_L^2}{r^8} + \mathcal{O}(1/r^{16}) + \cdots, \tag{31}$$

$$h(r) = 1 + \frac{h_L}{r^4} + \frac{405}{44}\frac{h_L^2}{r^8} + \mathcal{O}(1/r^{16}) + \cdots, \tag{32}$$

$$j(r) = 1 - \frac{3h_L}{r^4} - \frac{2835}{44}\frac{h_L^2}{r^8} + \mathcal{O}(1/r^{16}) + \cdots. \tag{33}$$

However, for $z = 3$ and with generic k, we get

$$f(r) = 1 + \frac{k}{2r^2} + \frac{127}{1352}\frac{k^2}{r^4} + \mathcal{O}(1/r^5) + \cdots, \tag{34}$$

$$g(r) = 1 + \frac{23}{676}\frac{k^2}{r^4} + \frac{12h_L}{r^5} + \mathcal{O}(1/r^6) + \cdots, \tag{35}$$

$$h(r) = 1 - \frac{3}{338}\frac{k^2}{r^4} + \frac{h_L}{r^5} + \mathcal{O}(1/r^6) + \cdots, \tag{36}$$

$$j(r) = 1 + \frac{9}{338}\frac{k^2}{r^4} - \frac{4h_L}{r^5} + \mathcal{O}(1/r^6) + \cdots, \tag{37}$$

where we have only one arbitrary parameter h_L characterizing both solutions at large r. Let us emphasize that the discrepancy between even and odd z follows from the expansion (29) we have considered. There may be fractional powers of x in the expansion (29) which can remedy the situation for the even z case. It is also possible that we have made an inappropriate choice of coordinates to discuss the solutions for large r. Nevertheless, we fix $z = 3$ in the numerical part of the calculations (see Sec. IV C), for the sake of clarity.

B. Series solution about the event horizon

Let us now focus on the series solution about the presumed horizon. In order to have a nonextremal black hole, g_{tt} and g_{rr} components of the metric (14) must have a simple zero and a simple pole (see Refs. [16] and [20]) at the finite horizon $r = R_0$. This assumption leads to the following horizon expansions of the functions,

[3]To keep the following discussion simple, we only present our findings for the $z = 2$ and $z = 3$ cases. The generic behavior of the solutions is captured by the $z = 2$ choice when z is even ($z = 4, 6, 8, \ldots$) or by the $z = 3$ choice when z is odd ($z = 5, 7, 9, \ldots$).

$$f(r) = \sqrt{r - R_0} \sum_{n=0}^{\infty} f_n (r - R_0)^n, \tag{38}$$

$$g(r) = \frac{1}{\sqrt{r - R_0}} \sum_{n=0}^{\infty} g_n (r - R_0)^n. \tag{39}$$

At this stage it is worthwhile to discuss the constraints on the gauge field functions at the horizon in order to construct the series expansion for the functions $h(r)$ and $j(r)$. These constraints can easily be seen from the general form of the field equations (21), (22), and (23) that we discussed in Sec. III. This set implies that the gauge field function $w(r)$ and its derivative must be related at the horizon as

$$w'(R_0) = \frac{w(R_0)(w^2(R_0) - k)}{(kR_0 - \frac{1}{2g_{\mathrm{YM}}^2 L^2}\frac{(w^2(R_0)-k)^2}{2R_0} - L^2 R_0^3 \Lambda)}, \tag{40}$$

which amounts to relating the expansion coefficients on the horizon

$$j(R_0) = j_0 = \frac{2h_0 R_0 (h_0^2 R_0^2 (z+1) - k)}{2kR_0 + R_0^3(z^2 + 2z + 3) - \frac{(z-1)(k - h_0^2 R_0^2 (z+1))^2}{R_0 (z+1)}}; \quad \text{for } z > 1, \tag{41}$$

where $w(R_0) = \sqrt{z+1} R_0 h_0$, with the definition $h_0 \equiv h(R_0)$. The subtle difference between the planar case and the other cases shows itself here. When $k = 0$, the horizon radius cancels out and j_0 depends only on h_0 and the dynamical exponent z. To make the meaning of h_0 clear, consider a noncoordinate basis for the one-forms [5]

$$\theta_t = L r^z f(r) dt, \quad \theta_{x_i} = L r dx^i,$$
$$\theta_r = L \frac{g(r)}{r} dr, \quad i = 1, 2, \tag{42}$$

in which the planar metric (14) takes the form $ds^2 = \eta^{\mu\nu} d\theta_\mu d\theta_\nu$, with $\eta^{\mu\nu} = \mathrm{diag}(-1, 1, 1, 1)$. The gauge connection simply follows as

$$A = \frac{\sqrt{z+1}}{L} h(r)(T^1 \theta_1 + T^2 \theta_2). \tag{43}$$

This suggests that h_0 can be considered as the strength of the gauge field at the horizon, up to some normalization. There is also an upper bound for the gauge field function $w(r)$ for a given horizon radius R_0, which follows from the condition for a regular horizon, i.e.,

$$\left.\frac{d\mu}{dr}\right|_{r=R_0} > 0. \tag{44}$$

Then, with the help of (23), one finds that

$$k - \frac{1}{2g_{\mathrm{YM}}^2 L^2}\frac{(w^2(R_0) - k)^2}{2R_0^2} - L^2 R_0^2 \Lambda > 0. \tag{45}$$

In terms of $w(R_0) = \sqrt{z+1} h_0$, this inequality further simplifies to

$$\frac{R_0^2 (z+1)(2k + R_0^2(3 + 2z + z^2))}{(z-1)} > (k - R_0^2 (z+1) h_0^2)^2. \tag{46}$$

The inequality (46) is rather important for numerical purposes. It weakly constrains the strength of the gauge field at the horizon, which in turn reduces the possible values for the shooting parameter h_0. For $k = 0$, h_0 is solely bounded by the z value. There is no dependence on the horizon radius; i.e., if a numerical solution is found for the system with a fixed value of h_0, then it will always remain a solution for different radii. On the other hand, for the other topologies where $k = \pm 1$, the gauge field strength changes with the changing horizon radius. The hyperbolic case $k = -1$ demands special attention regarding the value of the event horizon radius. By virtue of (45), there is a lower bound on the event horizon radius for fixed z:

$$|\Lambda| > \frac{1}{L^2 R_0^2}\left(1 + \frac{1}{4 g_{\mathrm{YM}}^2 R_0^2 L^2}\right). \tag{47}$$

The bound and the relations above can also be extracted from near horizon expansions. Assuming that the functions $h(r)$ and $j(r)$ are finite on the horizon, they read

$$h(r) = \sum_{n=0}^{\infty} h_n (r - R_0)^n, \tag{48}$$

$$j(r) = \sum_{n=0}^{\infty} j_n (r - R_0)^n. \tag{49}$$

Inserting the expansions (29), (48), and (49) into (25), (26), (27), and (28), one finds solutions depending on two free parameters h_0, the strength of the gauge field at the horizon, and R_0, the horizon radius for a fixed z value.

As a simple example, for $z = 2$ and $k = 0$, one gets

$$g_0 \to \frac{\sqrt{2R_0}}{\sqrt{11 - 3h_0^4}}, \tag{50}$$

$$j_0 \to \frac{6h_0^3}{11 - 3h_0^4}, \tag{51}$$

$$h_1 \to \frac{h_0(3h_0^4 + 6h_0^2 - 11)}{(11 - 3h_0^4)R_0}, \tag{52}$$

$$g_1 \to \frac{\sqrt{2}(18h_0^8 + 27h_0^6 - 99h_0^4 + 121)}{(11 - 3h_0^4)^{5/2}\sqrt{R_0}}, \tag{53}$$

$$f_1 \to \frac{f_0(-27h_0^8 + 9h_0^6 + 165h_0^4 - 242)}{(11 - 3h_0^4)^2 R_0}. \tag{54}$$

Note that all of the coefficients depend on two parameters: h_0 and R_0. Although f_0 appears to be a free parameter, it is in fact just an overall normalization factor, as was noted earlier in the penultimate paragraph of Sec. III. The bound on h_0 is now clear. In order to have real values for g_0, h_0 must be smaller than a value depending on z, and for $z = 2$ and $k = 0$, the strength of the gauge field must be $h_0^4 < 11/3$, which is consistent with (46). Finally, the value in (41) is also recaptured here.

To sum up, we have paved the way for numerical computation by finding the initial values for functions in terms of h_0 and R_0. Now, fixing one of the two parameters, namely the event horizon radius R_0, the shooting method can be used to search for numerical solutions. For a fixed value of R_0, we numerically evolve the functions and make them converge to unity at infinity by fine-tuning the initial value h_0. The behavior of solutions differs considerably for small and large horizon radius values, and it also depends on the topology.

C. Numerical solutions

We begin with the larger black holes and fix $z = 3$ in order to compare results for different values of k. For the numerical integration, MATLAB's differential equation solver ODE45 was used with default settings, which implements the Runge-Kutta method with variable step size and a relative tolerance value of 10^{-3} (with 0.1 accuracy). Convergence is obtained for sufficiently fine-tuned initial conditions specified at the horizon.

It turns out that there is a unique critical value of h_0, within the allowed region described by (46), where we have the desired asymptotics. This is quite different from what was observed in asymptotically flat or AdS analogues of these black holes, where solutions behave peculiarly depending on the horizon topology and the value of the cosmological constant. For example, spherically symmetric EYM black hole solutions with AdS asymptotics exist in continuous open intervals [28]—i.e., $0 < \omega_h < \omega_h^c$, where ω_h is the shooting parameter and ω_h^c is the critical value of the gauge field above which no solution exists. Moreover, the solutions we have found have no nodes—regardless of the topology—whereas in AdS for $k = 1$, the gauge fields have nodes for sufficiently small $|\Lambda|$ [28] and the solutions with $k = 0, -1$ are nodeless [29].

Setting $R_0 = 10$, we see from Figs. 1 and 2 that, for large black holes, the solutions behave similarly regardless of the topology of the event horizon. Although we plot the functions for all values of k, the graphs coalesce into one with a small difference between their shooting parameters h_0. The metric functions $f(r)$ and $g(r)$ start from zero and infinity, respectively, then converge to 1 monotonically. We have the following results for the initial value of the gauge field function, i.e., the shooting parameter

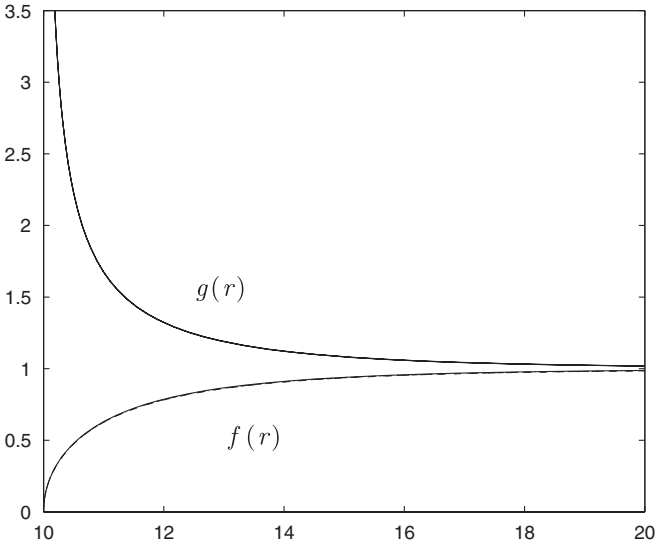

FIG. 1. The figure plots the metric functions $f(r)$ and $g(r)$ as a function of radius r. This is an example of a large black hole with $R_0 = 10$, where the plots overlap for all values of k.

$$h_0 = \begin{cases} 1.025530137 & \text{for } k = 1 \\ 1.023139854 & \text{for } k = -1 \\ 1.024335678 & \text{for } k = 0, \end{cases} \tag{55}$$

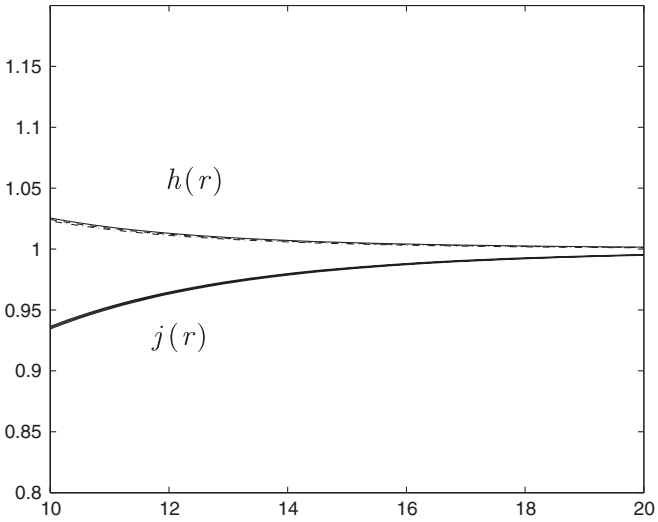

FIG. 2. The figure shows the gauge field functions $h(r)$ and $j(r)$ as a function of radius r with $R_0 = 10$. The initial values of functions for different topologies are very close to each other. Graphs for different topologies merge into one.

with the cutoff value $r_{\max} = 1000$. In order to extend the numerical integration to a larger distance, the shooting parameter h_0 must be fine-tuned. As an example, for $k = 1$ and $R_0 = 10$, setting $h_0 = 1.025530137219$ yields the desired asymptotics at $r_{\max} = 10.000$. The value of j_0 simply follows from (41).

We then fix $R_0 = 0.5$ in order to investigate the smaller black holes. The behavior of the solutions changes drastically. First of all, the functions of spherical and hyperbolic solutions decay appreciably slower and, moreover, the shooting parameters (i.e., h_0) differ considerably. From Figs. 3 and 4, we see that for the spherical case the metric function $f(r)$ makes a peak first and then converges to unity, unlike the planar and hyperbolic cases, where the functions monotonically converge to 1. The other metric function, $g(r)$, reaches a minimum and then approaches 1 for the spherically symmetric black holes. It turns out that for small black holes we have the following gauge field strengths (see Fig. 5):

$$h_0 = \begin{cases} 1.425617169 & \text{for } k = 1 \\ 0.278652475 & \text{for } k = -1 \\ 1.024335678 & \text{for } k = 0. \end{cases} \tag{56}$$

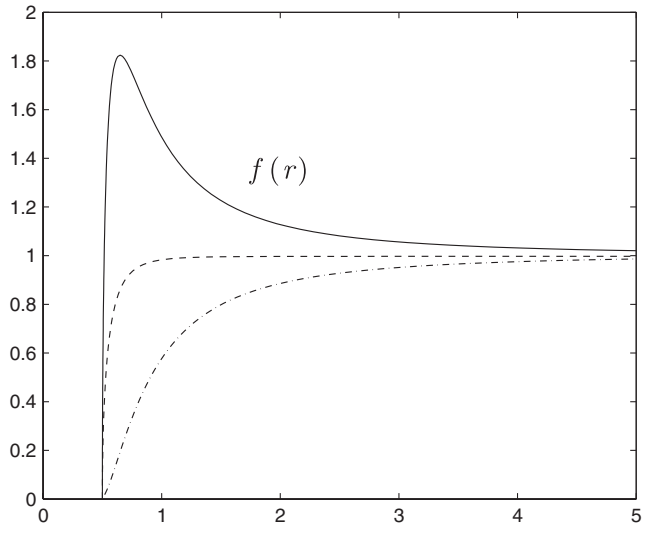

FIG. 3. A small black hole with $R_0 = 0.5$. The figure shows the metric function $f(r)$ for different cases $k = 1, -1, 0$. The solid line corresponds to $k = 1$, the dashed line to $k = 0$, and the dot-dashed line to $k = -1$, respectively.

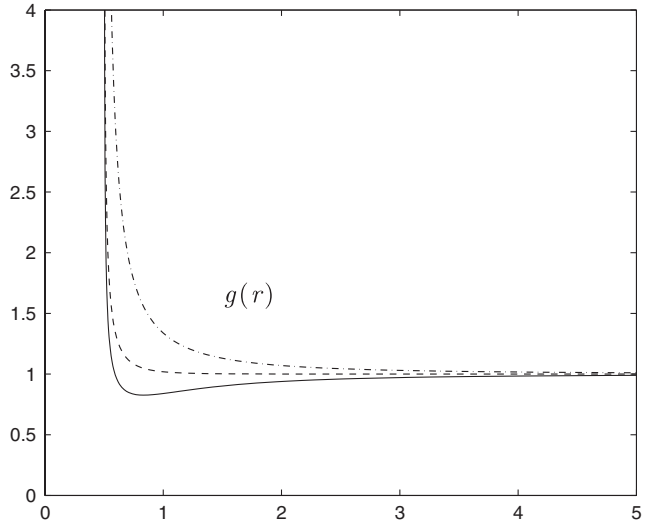

FIG. 4. The figure illustrates the metric function $g(r)$ with a small radius $R_0 = 0.5$. The solid line indicates $k = 1$, while the $k = 0$ and $k = 1$ cases are represented by dashed and dot-dashed lines, respectively.

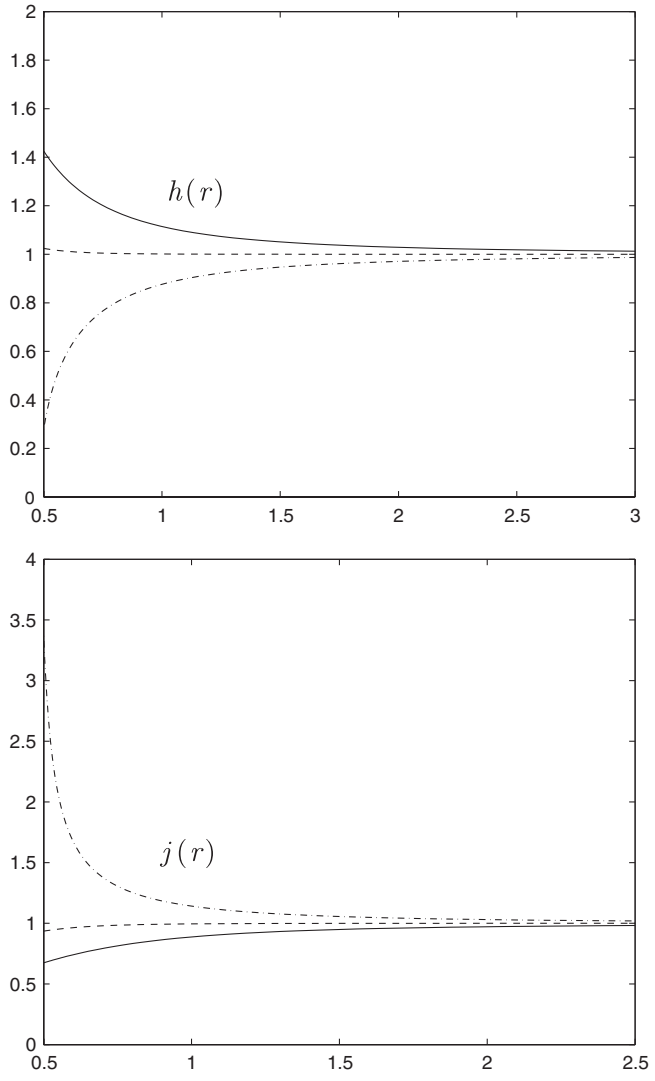

FIG. 5. The gauge field function $h(r)$ is displayed on the top and $j(r)$ at the bottom, both as functions of r. In both graphs, $R_0 = 0.5$. The solid line indicates $k = 1$, while the $k = 0$ and $k = 1$ cases are represented by dashed and dot-dashed lines, respectively.

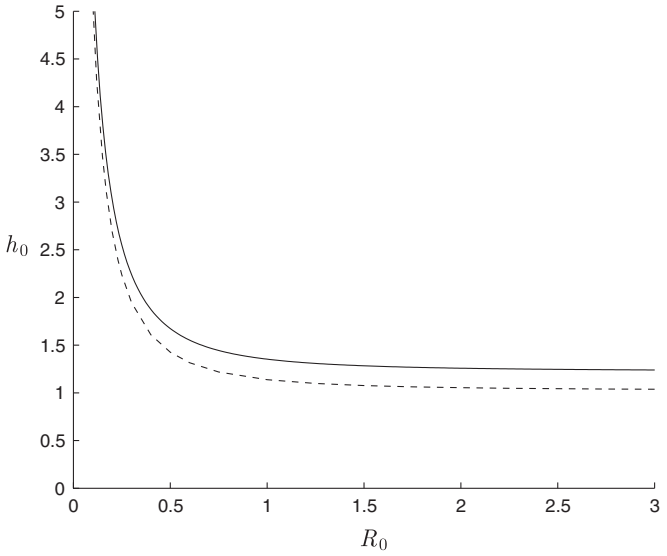

FIG. 6. The inequality (46) as a function of R_0 is plotted with a solid line for $k = 1$. The dashed line corresponds to the numerical values of h_0 as a function of R_0 for spherically symmetric black holes.

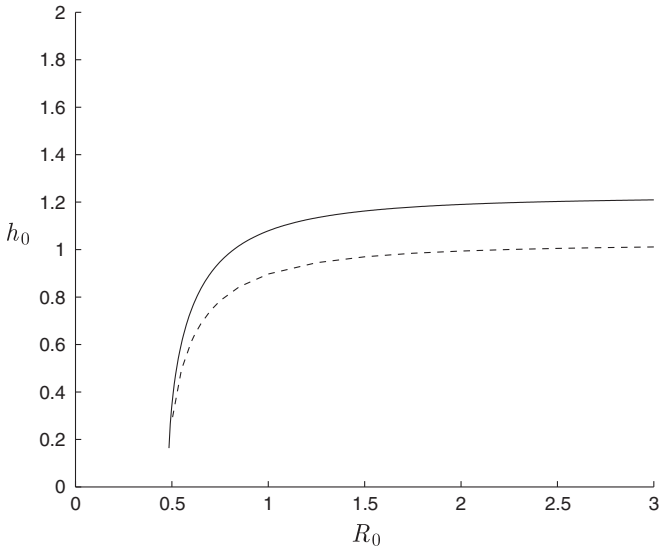

FIG. 7. The inequality (46) as a function of R_0 is plotted with a solid line for $k = -1$. The dashed line corresponds to the numerical values of h_0 as a function of R_0 for hyperbolically symmetric black holes. The lower bound (47) on the horizon radius is apparent.

Having seen the differences between large and small black holes, let us now compare the analytic bound (46) with the values of h_0 for different radii. For planar black holes, a unique value of h_0 is sufficient for all event horizon radii. Meanwhile, for the spherical case one needs larger gauge fields for small radii, and hyperbolic ones can support weaker gauge fields as the radius gets smaller. A similar behavior was observed for the Abelian field strength in the works of [16,20]. For clarity, we plot h_0 versus R_0 for both spherical (Fig. 6) and hyperbolic (Fig. 7) cases. The solid line depicts the solution of the inequality (46) as a function of R_0, and the dashed line represents the numerical values obtained from the shooting method. Evidently, the bound (46) is saturated as the horizon radius R_0 gets smaller. It is worth emphasizing that the lower limit on the horizon radius (47) for $z = 3$ is consistent with the numerical results; i.e., from Fig. 7 we see that there is no solution below $R_0 \sim 0.48$.

V. THERMAL BEHAVIOR

Finally, let us compute the temperature and discuss the thermal behavior of these black holes. We resort to the Euclidean metric obtained by a Wick rotation to compute the temperature, which leads to the following expression [17],

$$T = \frac{f_0 R_0^{z+1}}{4\pi g_0}, \tag{57}$$

where f_0 and g_0 are the expansion coefficients in the near horizon limit. The general expression from the series solution near the horizon determines g_0 in terms of k, h_0, R_0, and z:

$$g_0 = \frac{\sqrt{2(z+1)}R_0^{3/2}}{(2h_0^2 k R_0^2(z-1) + h_0^4 R_0^2(1-z)(z+1) - k^2\frac{(z-1)}{(z+1)} + 2k + R_0^2(3+2z+z^2))^{1/2}}. \tag{58}$$

Recall that the coefficient f_0 is to be determined from the normalization of the numerical solution, so it depends on the shooting parameter h_0. Therefore, fixing $z = 3$, the temperature now depends only on the horizon radius and the topology. After finding several numerical solutions for different R_0 values, we plot Fig. 8 by computing the temperature within the limits of numerical accuracy. It is clear from this figure that as the radius gets smaller, black holes get cooler at different rates. Hyperbolic ones have a higher cooling rate than planar ones, and the spherical black holes are hotter for small radii. In the large R_0 limit, the temperatures become identical just like the solutions. The thermal behavior of these black holes is the opposite of their AdS counterparts, where the Hawking

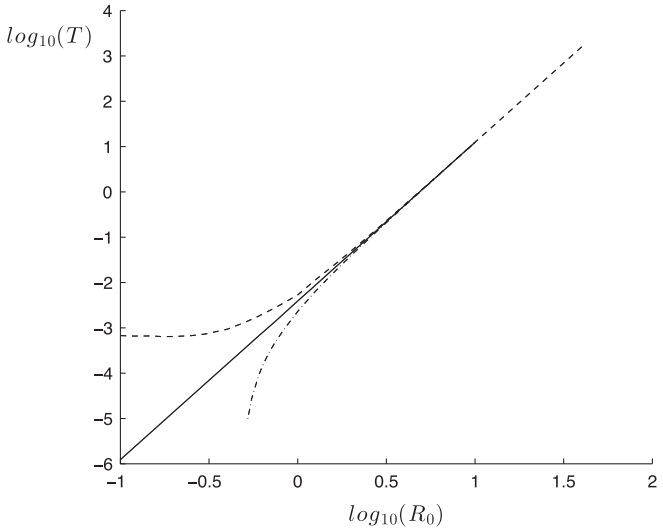

FIG. 8. Temperature versus horizon radius for $z = 3$. The different topologies are represented by a solid line $k = 0$, a dashed line $k = 1$, and a dot-dashed line $k = -1$.

temperature increases with the ever decreasing radius causing thermal instability. Moreover, it is clear that the EYM black holes do not exhibit Hawking-Page transition. A similar thermal behavior is observed for the Lifshitz black holes supported by Abelian p forms [16,20], which indicates that the black holes become extremal; i.e., they have zero Hawking temperature in the vanishing black hole size.

VI. CONCLUSIONS

In this work, we have studied the Lifshitz black holes with different horizon topologies in four-dimensional cosmological EYM theory. After obtaining the gauge field that supports the Lifshitz spacetime (2), we found numerical black hole solutions with different horizon topologies by suitably fine-tuning the gauge field strength at the horizon. Through the series solution of the field equations, we have found a quite interesting property: The geometries with odd z support black holes with different horizon topologies, whereas for even z only planar ones are supported. Thus we have fixed $z = 3$ in order to investigate all possible scenarios. From numerical results, we have observed that the behavior of solutions for different topologies changes considerably for small black holes, whereas it becomes identical for large horizon black holes. We have also analyzed the thermal behavior of the numerical solutions by computing the Hawking temperature for all types of black holes. We have found that there is a rapid decay in temperature as the black hole radius gets smaller and, moreover, black holes do not display Hawking-Page transition. In this respect, the EYM black holes and the Abelian counterparts [16,20] have quite similar characteristics, but they both differ considerably from their conformal cousins. The phenomenological models we discuss here and the ones with massive vectors [5,16] are not the only possibilities for Lifshitz spacetime. In string embedded constructions, soliton and black hole solutions with Lifshitz asymptotics are shown to exhibit phase transitions [36,37], which are analogous to the Hawking-Page transition in AdS. This discrepancy between the models calls for further study.

One of the most important questions to ask relates to the use of EYM theory in nonrelativistic holography. Certainly, Lifshitz spacetimes and black holes with non-Abelian matter sources deserve further attention. The finite temperature effects in a possible dual theory are expected to be mimicked by the black hole solutions, similar to the AdS Schwarzschild black hole in AdS/CFT correspondence. Also, as we have discussed in the Introduction, the holographic superconductor models with Lifshitz scalings employ black holes with non-Abelian fields in which these solutions can be useful. Although the holographic description of matter Lagrangians with Abelian and scalar fields has been studied to some extent, there has not been much work done on EYM theory in which these solutions can find a practical application.

A further direction of research would be to consider the extension of these black holes. First, the existence of analogous solutions can be considered by extending the $SU(2)$ symmetry Ansatz to higher spacetime dimensions. It would also be interesting to investigate the generalization of the gauge group $SU(2)$ to $SU(N)$. In another vein, here we have only considered a purely magnetic part; one could still extend this Ansatz by turning on the function $q(r)$ in (19) and looking for the existence of dyonic black holes. It would certainly be of interest if the non-Abelian counterparts of Lifshitz solitons [16,20,38] could be found.

ACKNOWLEDGMENTS

I thank Özgür Sarıoğlu for suggesting this problem and for his valuable comments and critical reading of the manuscript. I also thank Bayram Tekin, Dieter Van den Bleeken, and Robert Mann for their comments and suggestions, and Gökhan Alkaç and Ozan Tuğluk for their help in the numerical part of the calculations. I would also like to thank the anonymous referee for his useful comments and suggestions. This work is partially supported by Scientific and Technological Research Council of Turkey (TÜBİTAK) Grant No. 113F034.

APPENDIX

Here we give the expression for the Kretschmann scalar of the metric for generic z and k:

$$R_{\mu\nu\alpha\lambda}R^{\mu\nu\alpha\lambda} = \frac{4}{L^4 g(r)^6}\left(\frac{2g(r)^2(rf'(r)+zf(r))^2}{f(r)^2} + \frac{kg(r)^4(kg(r)^2-2r^2)}{r^4} + g(r)^2 + 2(g(r)-rg'(r))^2\right) + \frac{4}{L^4 g(r)^6}\left(\frac{(r(g(r)(rf''(r)+(2z+1)f'(r))-rf'(r)g'(r))+zf(r)(zg(r)-rg'(r)))^2}{f(r)^2}\right). \tag{A1}$$

In order to check the regularity of (A1) at the horizon, we first fix $z = 3$ and plug the horizon expansions (39) into (A1). A quick check at the lowest order shows that the scalar is finite at the horizon, and further computation yields

$$R_{\mu\nu\alpha\lambda}R^{\mu\nu\alpha\lambda}|_{r=R_0} = \frac{f_0^2(4g_0^6k^2 + g_1^2R_0^8 - 20g_0g_1R_0^7 + 104g_0^2R_0^6) + 9f_1^2g_0^2R_0^8 - 6f_0f_1g_0R_0^7(g_1R_0 - 10g_0)}{f_0^2g_0^6L^4R_0^4}. \tag{A2}$$

For the regularity of the Kretschmann scalar at the far field, first perform the transformation in Sec. IV A:

$$R_{\mu\nu\alpha\lambda}R^{\mu\nu\alpha\lambda} = \frac{4}{L^4 g(x)^6}\left(\frac{2g(x)^2(-xf'(x)+zf(x))^2}{f(x)^2} + kg(x)^4\left(kg(x)^2 - \frac{2}{x^2}\right)x^4 + g(x)^2\right) + \frac{4}{L^4 g(x)^6}\left(\frac{((g(x)(x^3f''(x)+2x^2f'(x)-(2z+1)x^2f'(x))-x^3f'(x)g'(x))+zf(x)(zg(x)+xg'(x)))^2}{xf(x)^2}\right) + \frac{4}{L^4 g(x)^6}(2(g(x)+xg'(r))^2). \tag{A3}$$

Employing expansions (29) in (A3) and taking the limit $x \to 0$,

$$\lim_{x\to 0} R_{\mu\nu\alpha\lambda}R^{\mu\nu\alpha\lambda} = \frac{408}{g_0^4L^4}. \tag{A4}$$

[1] K. Balasubramanian and J. McGreevy, Phys. Rev. Lett. **101**, 061601 (2008).
[2] S. A. Hartnoll, Classical Quantum Gravity **26**, 224002 (2009).
[3] D. T. Son, Phys. Rev. D **78**, 046003 (2008).
[4] A. Adams, K. Balasubramanian, and J. McGreevy, J. High Energy Phys. 11 (2008) 059.
[5] S. Kachru, X. Liu, and M. Mulligan, Phys. Rev. D **78**, 106005 (2008).
[6] E. Ayon-Beato, A. Garbarz, G. Giribet, and M. Hassaine, J. High Energy Phys. 04 (2010) 030.
[7] M. Taylor, arXiv:0812.0530.
[8] J. Tarrio and S. Vandoren, J. High Energy Phys. 09 (2011) 017.
[9] R.-G. Cai, Y. Liu, and Y.-W. Sun, J. High Energy Phys. 10 (2009) 080.
[10] E. Ayon-Beato, A. Garbarz, G. Giribet, and M. Hassaine, Phys. Rev. D **80**, 104029 (2009).
[11] O. Sarioglu, Phys. Rev. D **84**, 127501 (2011).
[12] E. J. Brynjolfsson, U. H. Danielsson, L. Thorlacius, and T. Zingg, J. Phys. A **43**, 065401 (2010).
[13] K. Balasubramanian and J. McGreevy, Phys. Rev. D **80**, 104039 (2009).
[14] D.-W. Pang, J. High Energy Phys. 01 (2010) 116.
[15] G. Bertoldi, B. A. Burrington, and A. Peet, Phys. Rev. D **80**, 126003 (2009).
[16] U. H. Danielsson and L. Thorlacius, J. High Energy Phys. 03 (2009) 070.
[17] M. H. Dehghani, R. B. Mann, and R. Pourhasan, Phys. Rev. D **84**, 046002 (2011).
[18] W. G. Brenna, M. H. Dehghani, and R. B. Mann, Phys. Rev. D **84**, 024012 (2011).
[19] M. H. Dehghani and R. B. Mann, J. High Energy Phys. 07 (2010) 019.
[20] R. B. Mann, J. High Energy Phys. 06 (2009) 075.
[21] S. S. Gubser and S. S. Pufu, J. High Energy Phys. 11 (2008) 033.
[22] S. S. Gubser, Phys. Rev. Lett. **101**, 191601 (2008).
[23] J.-W. Lu, Y.-B. Wu, P. Qian, Y.-Y. Zhao, and X. Zhang, arXiv:1311.2699.
[24] R. Bartnik and J. McKinnon, Phys. Rev. Lett. **61**, 141 (1988).
[25] P. Bizon, Phys. Rev. Lett. **64**, 2844 (1990).
[26] P. Breitenlohner, P. Forgacs, and D. Maison, Commun. Math. Phys. **163**, 141 (1994).
[27] M. S. Volkov and D. V. Gal'tsov, Phys. Rep. **319**, 1 (1999).
[28] E. Winstanley, Classical Quantum Gravity **16**, 1963 (1999).
[29] J. J. Van der Bij and E. Radu, Phys. Lett. B **536**, 107 (2002).
[30] M. Basler, J. Phys. A **18**, 3087 (1985).
[31] M. Basler and A. Hadicke, Report No. JENA-N/84/20.
[32] P. Forgacs and N. S. Manton, Commun. Math. Phys. **72**, 15 (1980).

[33] P. G. Bergmann and E. J. Flaherty, J. Math. Phys. (N.Y.) **19**, 212 (1978).
[34] E. Witten, Phys. Rev. Lett. **38**, 121 (1977).
[35] D. V. Galtsov and A. A. Ershov, Phys. Lett. A **138**, 160 (1989).
[36] I. Amado and A. F. Faedo, J. High Energy Phys. 07 (2011) 004.
[37] B. Way, Phys. Rev. D **86**, 086007 (2012).
[38] R. Mann, L. Pegoraro, and M. Oltean, Phys. Rev. D **84**, 124047 (2011).